Magnetism, phase composition, and hyperfine fields of melt-spun Nd-Fe-B alloys with a few percent of neodymium

Zhao-hua Cheng and Bao-gen Shen
State Key Laboratory of Magnetism, Institute of Physics, Chinese Academy of Sciences
P.O. Box 603, Beijing 100080, Peoples Republic of China

Ming-xi Mao, Ji-jun Sun, Yi-de Zhang, and Fa-shen Li
Department of Physics, Lanzhou University, Lanzhou 730000, Peoples Rebpublic of China
(Received 23 January 1995; revised manuscript received 4 May 1995)

It is possible that melt-spun Nd-Fe-B alloys with a few percent of neodymium can be used as a raw material for inexpensive and bonded permanent magnets. After an appropriate heat treatment, melt-spun $Nd_4Fe_{77.5}B_{18.5}$ alloy has a coercive field of 3 kOe, a remanent magnetization of 12.5 kG, and an energy product of 13 MG Oe. However, at present, there is some debate on the origin of its hard magnetic properties. In the present work, the phase composition, magnetism, and hyperfine fields of melt-spun Nd-Fe-B alloys are studied. The effect of rare-earth element substitution for Nd, such as Pr, Gd, and Dy, on ^{11}B and ^{57}Fe magnetic hyperfine fields is also investigated. On the basis of the experimental results, the origin of the hard magnetic properties is discussed. The results indicate that (1) the melt-spun Nd-Fe-B alloys with a low Nd concentration annealed under an optimal heat treatment consist of body-centered-tetragonal Fe_3B (bct-Fe_3B) and a few percent of α-Fe and no $Nd_2Fe_{14}B$ magnetically hard phase; (2) about 5 at. % Fe atoms in $Fe_{III}(8g)$ site of bct-Fe_3B are replaced by Nd atoms in the samples annealed under optimal condition. NMR radio frequency (rf) enhancement effect results demonstrate that bct-Fe_3B containing Nd atoms has better permanent magnetic properties; (3) the substitution of some rare-earth elements, such as Pr, Gd, and Dy, does not influence the hyperfine field for ^{57}Fe in α-Fe; however, the hyperfine field for ^{11}B in bct-Fe_3B increases with the addition of Gd or Dy. Thus, it can be concluded that the hard magnetic properties of melt-spun Nd-Fe-B with a few percent of neodymium result from bct-Fe_3B containing Nd atoms, and not from the presence of the $Nd_2Fe_{14}B$ magnetically hard phase.

I. INTRODUCTION

The crystallization and macroscopic magnetic properties of melt-spun Nd-Fe-B alloys with a small Nd content have been investigated for several years.[1–6] However, the detailed crystallization products and the relationships between microscopic structure and the magnetic properties have not been fully understood. It was found that $Nd_4Fe_{77.5}B_{18.5}$ melt-spun ribbons showed a coercivity of 3 kOe, a magnetic remanence of 12.5 kG, and an energy product of 13 MG Oe at room temperature after an appropriate heat treatment. It can be used as inexpensive raw material for bonded magnets owing to the lower rare-earth Nd concentration. However, there are two different points of view on the origin of the hard magnetic properties. Previous work assumed that the $Nd_2Fe_{14}B$ magnetically hard phase was still present in the samples with low Nd content and the large coercivity was related to the presence of the $Nd_2Fe_{14}B$ phase on the basis of magnetic phase analysis. However, recent nuclear magnetic resonance (NMR) and Mössbauer effect (ME) experiments have demonstrated that the magnetically hard $Nd_2Fe_{14}B$ phase does not exist in these samples.[7,8] Furthermore, NMR and ME results indicate that the hard magnetic properties originate from the existence of body-centered-tetragonal Fe_3B (bct-Fe_3B) containing Nd atoms. Since there are certain characteristics of the bct-Fe_3B microscopic structure and that of $Nd_2Fe_{14}B$, mixtures of Fe_3B and $Nd_2Fe_{14}B$ are good systems to explore the effect of the various phase components on the magnetic properties. A series of studies which combined microscopic techniques, such as NMR and ME, and magnetization measurements and x-ray diffraction (XRD) have been directed toward the understanding of this mechanism.

II. EXPERIMENTAL DETAILS

Raw materials of iron (99.9% in purity), rare-earth metal R (R = Pr, Nd, Gd, and Dy, 99.9%), and Fe-B alloy (98.6%) were arc melted into homogeneous buttons with the nominal composition. Amorphous ribbons were prepared by melt spinning in a high-purity argon atmosphere with a speed of 47 m/s. The thickness and width of the ribbons were about 20 μm and 1 mm, respectively. XRD patterns confirmed the amorphous state of the ribbons. The as-quenched ribbons were annealed in steel capsules evacuated to 2×10^{-5} Torr using different heat treatment conditions. Hysteresis loop measurements on the crystallized samples were carried out at room temperature using a vibrating sample magnetometer with a maximum magnetic field of 15 kOe. XRD experiments were

performed with Co $K\alpha$ radiation.

Zero-field spin-echo NMR spectra of ^{11}B and ^{57}Fe were obtained at a temperature of 8 K for frequencies ranging from 20 to 60 MHz. A closed-cycle refrigerator was employed to provide this low temperature without the consumption of liquid helium. The temperature was measured at the surface of the samples. The powder samples were mixed with a thermal-conducted adhesive and then glued to the end of the refrigerator. The pulse sequence 1.5-60-1.5 μs at a given amplitude was applied to obtain the maximum spin-echo signal. The spin-lattice relaxation time T_1 and spin-spin relaxation time T_2 for the various peaks were determined by measuring the spin-echo intensity versus the pulse repetition time and the separation time between two pulses, respectively. The spin-echo amplitude was calibrated by a rf pulse standard with the same frequency as that of spin-echo signal; both were recorded and accumulated many times using a computer. The Mössbauer spectra were recorded at room temperature using a constant-acceleration spectrometer with a $^{57}Co(Pd)$ source. The isomer shifts (IS's) given in this paper were relative to α-Fe at room temperature.

III. EXPERIMENTAL RESULTS

A. Effect of Nd content and heat treatment on the hard magnetic properties

Since Fe_3B is a magnetically soft phase and $Nd_2Fe_{14}B$ is a magnetically hard phase, we prepare a series of alloys with the composition of $(Fe_3B)_{1-x}(Nd_2Fe_{14}B)_x$, corresponding to $x=0.17$, 0.26, 0.34, 0.42, 0.65, 0.78, and 1.0, to investigate the effect of Nd content on the hard magnetic properties. The as-quenched ribbons are magnetically soft with a coercivity of less than 10 Oe. When the samples are annealed above crystallization temperature for 2 min, the coercivity increases rapidly with increasing annealing temperature. T_a, reaching a maximum, then decreases monotonically. The temperature dependence of the intrinsic coercivity ${}_iH_c$ shows that the temperature about 650–700 °C is the optimal annealing temperature, as shown in Fig. 1. It is noteworthy that for temperatures above 650 °C, the annealing has a different effect on the coercivity for different compositions. The annealing temperature dependence of ${}_iH_c$ has a little variation for compositions near $Nd_2Fe_{14}B$ and goes through a sharp maximum to lower values for compositions near Fe_3B. This result implies that the crystallization products at different temperatures vary for low Nd and high Nd concentration melt-spun Nd-Fe-B alloys. The detailed effect of heat treatments on the magnetic properties and phase composition will be discussed in the next section.

The concentration dependence of the intrinsic coercivity ${}_iH_c$ and energy product $(BH)_{max}$ obtained at optimal annealing temperature is shown in Figs. 2(a) and 2(b), respectively. It is apparent that for $x>0.5$, both the coercivity and energy products increase monotonically with increasing x; for $x<0.5$, the coercivity exhibits high values of 2.5–3.0 kOe in alloys with $0.26\le x\le 0.42$. Large $(BH)_{max}$ values are obtained within a narrow concentration range near $x=0.34$.

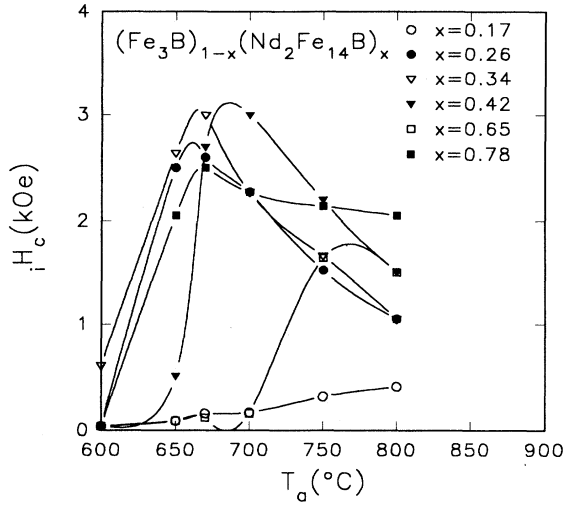

FIG. 1. Intrinsic coercivities ${}_iH_c$ of $(Fe_3B)_{1-x}(Nd_2Fe_{14}B)_x$ alloys as a function of annealing temperature T_a for 2 min.

B. The development of phase composition

1. X-ray diffraction results

All as-quenched ribbons are in the amorphous state. When they are annealed at 650–700 °C for 2 min, XRD patterns demonstrate that the samples with higher Nd concentration consist of $Nd_2Fe_{14}B$ and $Nd_{1.1}Fe_4B_4$, with a small amount of α-Fe also present; the samples with

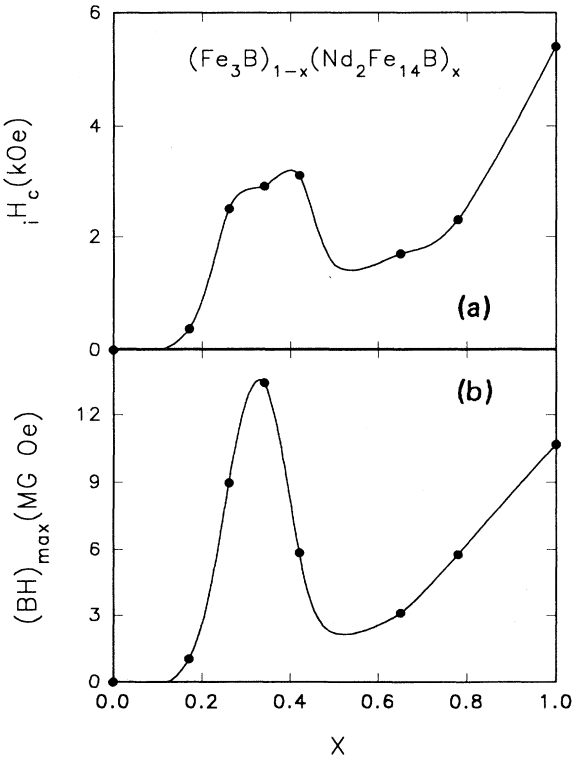

FIG. 2. The concentration dependence of (a) optimal intrinsic coercivity ${}_iH_c$ and (b) energy product $(BH)_{max}$.

lower Nd concentration are found to contain a mixture of bct-Fe_3B and a few percent of α-Fe and without the existence of $Nd_2Fe_{14}B$ (Fig. 3).

Since the samples with low Nd content consist of the Fe_3B metastable phase, the sample of $Nd_4Fe_{77.5}B$ was selected to study the effect of heat treatment on the phase composition. This alloy corresponds to the composition with $x=0.34$ investigated previously. The as-quenched ribbons of $Nd_4Fe_{77.5}B_{18.5}$ were annealed between 600 and 950 °C resulting in different crystalline phases. XRD patterns (Fig. 4) show that the samples annealed at temperatures in the range 600–800 °C for 2–300 min consist of only the bct-Fe_3B metastable phase and a few percent of α-Fe. At 670 °C, the annealing times between 2 and 300 min do not influence the phase composition, but only increase the crystallites' sizes. For the sample annealed at 839 °C for 60 min, a paramagnetic $Nd_{1.1}Fe_4B_4$ phase appears along with bct-Fe_3B and α-Fe. When the annealing temperature is higher than 850 °C for 60 min, the metastable phase Fe_3B decomposes into Fe_2B and α-Fe. The sample annealed at 960 °C for 60 min constitutes $Nd_2Fe_{14}B$, $Nd_{1.1}Fe_4B_4$, Fe_2B, and α-Fe.

2. *NMR and ME results*

Both the NMR and ME results are consistent with XRD. For the samples with $x \geq 0.65$, the NMR spectra show a very intense peak and two weak peaks centered at 42.4, 48.5, and 46.7 MHz, respectively [Fig. 5(a)]. The resonance peak centered at 46.7 MHz is attributed to ^{57}Fe in bcc α-Fe. The peaks located at 42.4 and 48.5 MHz are attributed to ^{11}B and ^{57}Fe nuclei in the 16 k_2

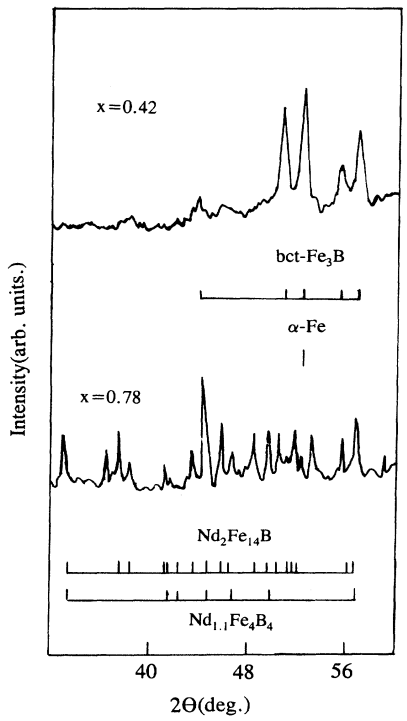

FIG. 3. XRD patterns of $(Fe_3B)_{1-x}(Nd_2Fe_{14}B)_x$ alloys annealed at 670 °C for 2 min. (a) $x=0.78$ and (b) $x=0.34$.

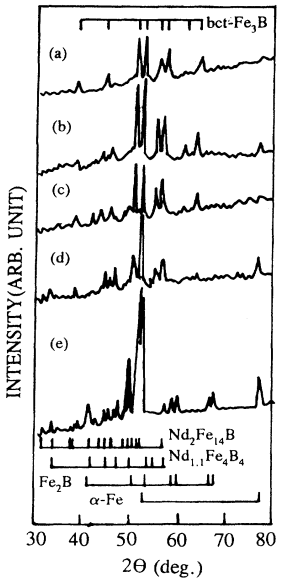

FIG. 4. XRD patterns of $Nd_4Fe_{77.5}B_{18.5}$ alloy annealed at different temperatures. (a) 670 °C for 2 min, (b) 670 °C for 300 min, (c) 800 °C for 2 min, (d) 839 °C for 60 min, and (e) 950 °C for 60 min.

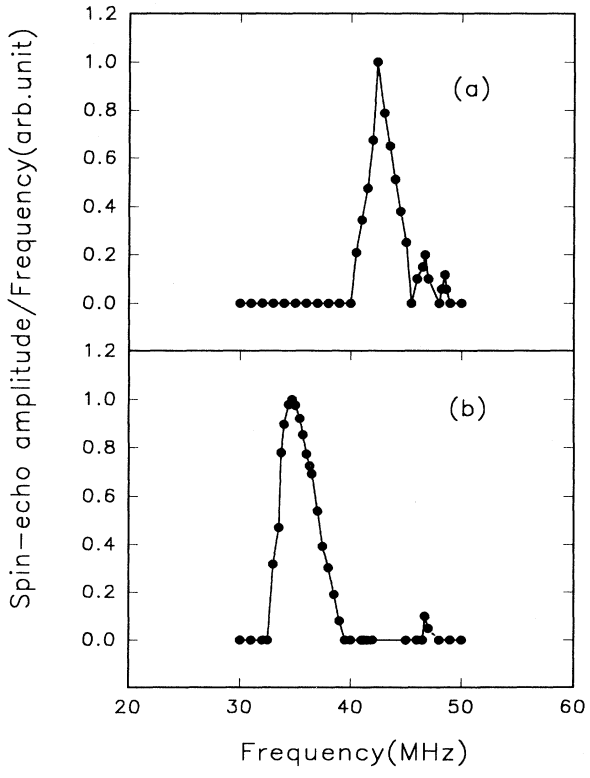

FIG. 5. NMR spectra of $(Fe_3B)_{1-x}(Nd_2Fe_{14}B)_x$ alloys annealed at 670 °C for 2 min. (a) $x=0.78$ and (b) $x=0.42$.

site of $Nd_2Fe_{14}B$. As we have discussed in previous work,[7-9] the resonance peaks originating from ^{57}Fe in the 4*e*, 4*c*, $16k_1$, and $8j_1$ sites occur between 41 and 47 MHz and are covered by the strong ^{11}B resonance peak located at 42.4 MHz. The signals at 52.0 and 53.0 MHz which arose from ^{57}Fe in $8j_2$ sites are two weak to be detected by NMR at 8 K. Therefore, the peaks at 42.4 and 48.5 MHz are characteristic of the $Nd_2Fe_{14}B$ magnetically hard phase. The Mössbauer spectra of the samples with $x \geq 0.65$ are fit with seven sextets and one doublet. The doublet, with a quadrupole splitting (QS) of 0.559 mm/s, corresponds to the $Nd_{1.1}Fe_4B_4$ paramagnetic phase on the basis of its hyperfine parameter and XRD data. One sextet with a hyperfine field (HF) of 331 kOe is obviously associated with α-Fe. The six sextets with hyperfine fields (HF's) of 350, 320, 282, 279, 252, and 248 kOe are attributed to ^{57}Fe in the $8j_2$, $16k_1$, $8j_1$, $16k_2$, 4*c*, and 4*e* sites, respectively. The hyperfine fields are in agreement with those of previous work,[10-12] and the relative intensities are proportional to the on-site occupancies of the Fe atoms. For example, Fig. 6(a) shows the Mössbauer spectrum of the sample with $x = 1$. In the case of a magnetically ordered solid, the direction of the atomic magnetic moment is fixed due to the exchange interaction, and so is the HF direction. Hyperfine fields at nuclei of ferromagnetic materials are as large as 10^5 Oe for 3*d* elements and 10^7 Oe for 4*f* elements. The hyperfine interaction becomes the dominant factor producing the splitting of nuclear energy levels. Thus, NMR can detect the ferromagnetic materials without any external magnetic field and the NMR spectra of magnetically ordered materials reflect the HF distributions. However, in the case of the paramagnetic state of a solid, the direction of the hyperfine field varies randomly due to thermal motion of the *d* electrons with frequencies much higher than typical NMR frequencies. Therefore, the hyperfine interaction has a much reduced effect and the NMR frequency of paramagnetic substance is mainly determined by the externally applied magnetic fields. Since our NMR data are measured without any externally applied magnetic field, the paramagnetic $Nd_{1.1}Fe_4B_4$ phase is not observed by spin-echo NMR. The Mössbauer effect, however, can detect the existence of a paramagnetic phase on the basis of quadrupole splitting. Thus, a combined NMR and Mössbauer study can yield a more complete picture.

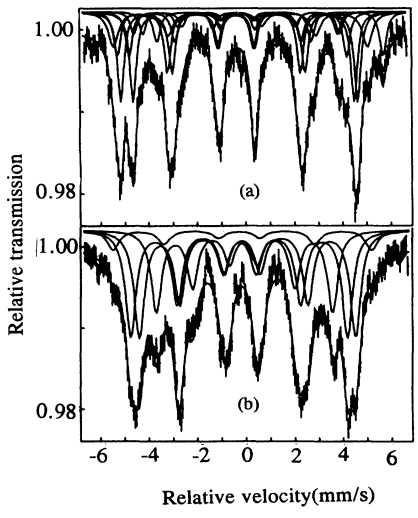

FIG. 6. Mössbauer spectra of $(Fe_3B)_{1-x}(Nd_2Fe_{14}B)_x$ alloys annealed at 670 °C for 2 min. (a) $x = 1.0$ and (b) $x = 0.42$.

NMR spectra [Fig. 5(b)] obtained from samples with $x \leq 0.42$ and annealed at 670 °C for 2 min show a strong peak and a weak peak centered at 34.7 and 46.7 MHz, respectively.[13] There is no trace of the characteristic $Nd_2Fe_{14}B$ peaks at 42.4 and 48.5 MHz. Although boron is not the major component in the $Nd_2Fe_{14}B$ phase, the natural abundance of ^{11}B is large (80.8%) and the relative NMR sensitive to the ^{11}B nucleus is very favorable. We note that the ^{11}B signal from the $Nd_2Fe_{14}B$ phase does not overlap that from bct-Fe_3B owing to the very large difference of HF values at B sites for these two phases. Thus, these phases can be clearly detected by NMR.

ME spectra from the samples with a low Nd concentration are consistent with NMR and XRD [Fig. 6(b)]. It is true that the complex Mössbauer spectra are difficult to decompose and can be fit in more than one way. We try to fit these spectra by various methods, but it is impossible to add the sextets corresponding to $Nd_2Fe_{14}B$ into these spectra. The best method is to fit these spectra using four sextets. The sextet with HF value of 331 kOe corresponds to α-Fe. The others with HF values of 288, 266, and 224 kOe are assigned to the ^{57}Fe nuclei in the three nonequivalent sites of bct-Fe_3B on the basis of HF values reported in an earlier work.[14] The fitting results are in agreement with that of $Nd_3Fe_{81}B_{16}$.[15]

It is well known that structural information can be obtained from either x-ray diffraction or hyperfine field techniques. However, since XRD is only sensitive to a well-developed phase, information concerning the B and Fe site occupancy as well as the microstructure of these alloys is not really available. Although previous work assumed that the $Nd_2Fe_{14}B$ phase is still present in the samples with low Nd content, the atomic ordering in the $Nd_2Fe_{14}B$ lattice might be far from perfect and its grain too small to be resolved by XRD. Consequently, there is a lack of direct evidence. Both NMR and Mössbauer measurements can provide the local information about the near-neighbor environment of detected nuclei. When there exists a certain short-range order in the near-neighbor environment of the B atoms, about 10–100 Å, it can be detected by NMR. In this way, it can identify the phases whose dimensions are too small for XRD techniques. Both NMR and ME show that there is no evidence for the presence of the $Nd_2Fe_{14}B$ magnetically hard phase.

The phases observed by XRD, NMR, and ME are listed in Table I. These results are similar to those for $(Fe_{1-x}Nd_x)_{81.5}B_{18.5}$ alloys.[9,16] However, the metastable phase $Nd_2Fe_{23}B_3$ is not found in the series reported here. Figure 7 illustrates the ternary Nd-Fe-B phase diagram corresponding to varying mixtures of Fe_3B and $Nd_2Fe_{14}B$.

The Mössbauer spectrum from as-quenched

TABLE I. The phase composition of $(Fe_3B)_{1-x}(Nd_2Fe_{14}B)_x$ alloys annealed 670 °C for 2 min.

	As-quenched	Crystallization products
$x=0.17$	Amorphous	$Fe_3B+\alpha$-Fe
$x=0.26$	Amorphous	$Fe_3B+\alpha$-Fe
$x=0.34$	Amorphous	$Fe_3B+\alpha$-Fe
$x=0.42$	Amorphous	$Fe_3B+\alpha$-Fe
$x=0.65$	Amorphous	$Nd_2Fe_{14}B+Nd_{1.1}Fe_4B_4+\alpha$-Fe
$x=0.78$	Amorphous	$Nd_2Fe_{14}B+Nd_{1.1}Fe_4B_4+\alpha$-Fe
$x=1.0$	Amorphous	$Nd_2Fe_{14}B+\alpha$-Fe

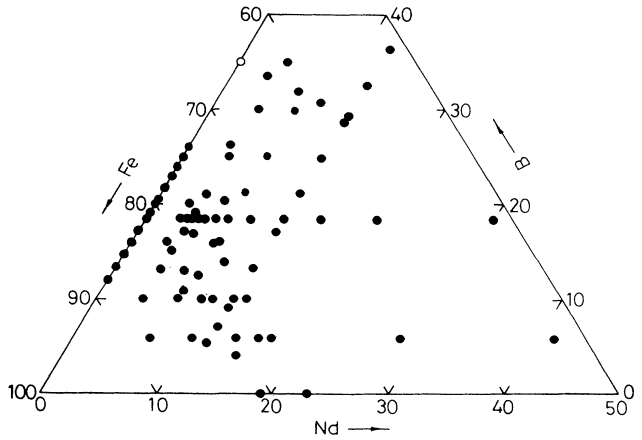

FIG. 7. Ternary phase diagram for Nd-Fe-B system showing the compositions investigated.

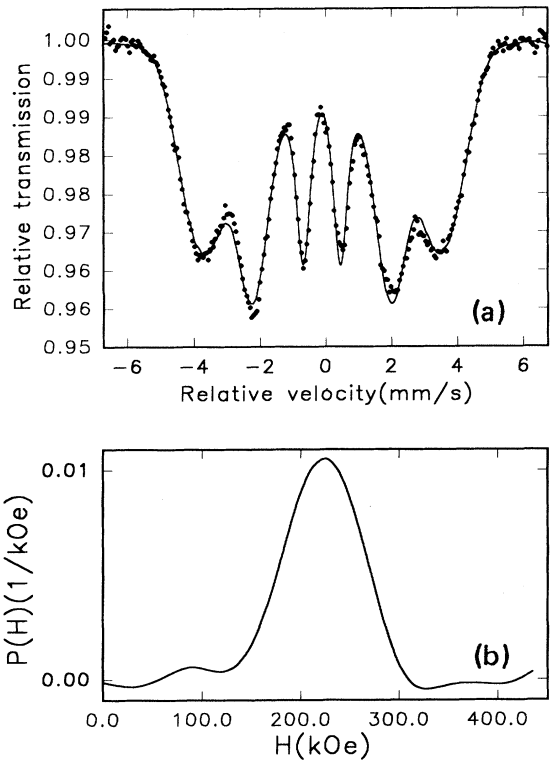

FIG. 8. (a) Mössbauer spectrum and (b) ^{57}Fe hyperfine field distribution $P(H)$ from the $Nd_4Fe_{77.5}B_{18.5}$ amorphous alloy.

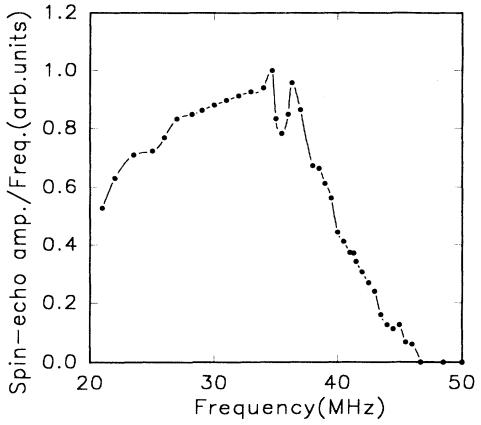

FIG. 9. NMR spectrum from the $Nd_4Fe_{77.5}B_{18.5}$ amorphous alloy.

$Nd_4Fe_{77.5}B_{18.5}$ ribbon is a typical amorphous broad sextet with a peak hyperfine field of 225 kOe and an average hyperfine field of 218 kOe [Fig. 8(a)]. The broad sextet and corresponding hyperfine field distribution $P(H)$ with only a single peak and without structure details cannot provide the information concerning the types of short-range order [Fig. 8(b)]. The NMR spectrum, however,

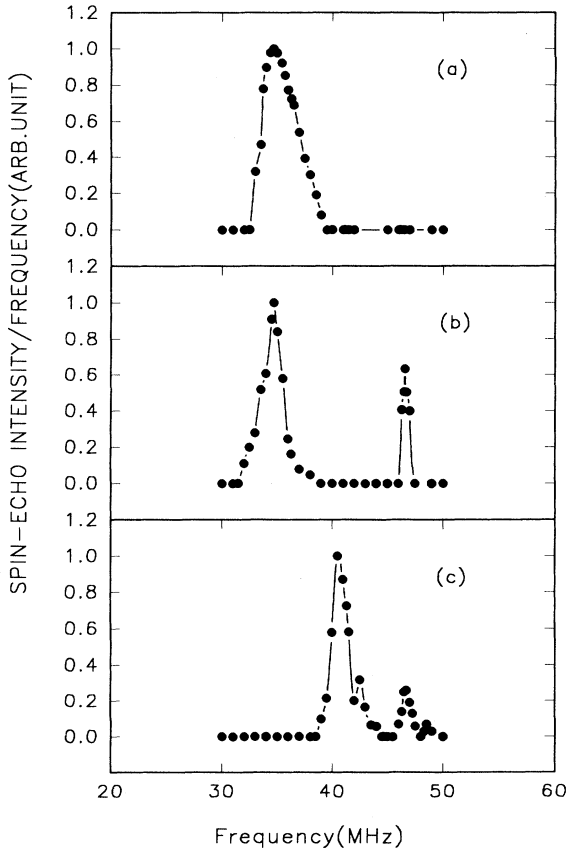

FIG. 10. NMR spectra of $Nd_4Fe_{77.5}B_{18.5}$ alloy annealed at different temperatures. (a) 670 °C for 2 min, (b) 839 °C for 60 min, and (c) 960 °C for 60 min.

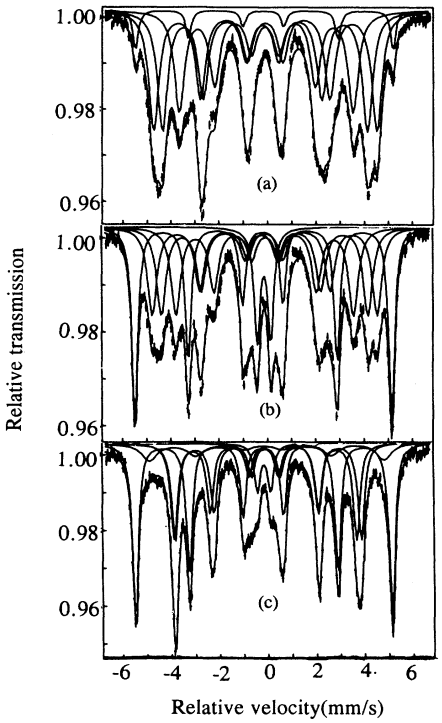

FIG. 11. Mössbauer spectra of $Nd_4Fe_{77.5}B_{18.5}$ alloy annealed at different temperatures. (a) 670 °C for 2 min, (b) 839 °C for 60 min, and (c) 960 °C for 60 min.

directly indicates that there are two resonance peaks centered at 34.7 and 36.3 MHz, respectively (Fig. 9). According to previous NMR studies on Fe-B-C amorphous alloys, these two peaks are attributed to ^{11}B in bct-Fe_3B and orthorhombic Fe_3B-like short-range orders, respectively.[17] This result gives clear evidence that the types of short-range order in amorphous alloys can be obtained by NMR more directly than by the Mössbauer effect and x-ray diffraction.

Figures 10 and 11 illustrate NMR and ME spectra from $Nd_4Fe_{77.5}B_{18.5}$ alloys annealed after the various heat treatments. The fit of the Mössbauer spectra and the assignments of NMR peaks have been discussed in previous work.[7,8] In many cases, both measurements give the same results as those of XRD experiments. The $Nd_{1.1}Fe_4B_4$ paramagnetic phase is not detected by NMR. The crystallization products of the $Nd_4Fe_{77.5}B_{18.5}$ alloy after the various heat treatments are listed in Table II.

IV. DISCUSSION

A. Effect of phase composition on the hard magnetic properties

Room-temperature hysteresis loops of the as-quenched samples have been measured. It was found that the amorphous ribbon is magnetically soft due to the lack of long-range-order magnetocrystalline anisotropy. When the samples are annealed above the crystallization temperature, their coercive fields increase rapidly, first with increasing annealing temperature T_a, reaching a broad maximum value, then decrease monotonically, as shown in Fig. 1. The larger coercive fields for high Nd concentration alloys is obviously due to the presence of the $Nd_2Fe_{14}B$ magnetically hard phase with very fine crystallite sizes and some minor phases which precipitate at grain boundaries and have a domain wall pinning effect. The low Nd content samples are found to contain no $Nd_2Fe_{14}B$, whereas the sample of $Nd_4Fe_{77.5}B_{18.5}$ exhibits a higher coercivity of 3 kOe. This implies that the large coercivity for low Nd content samples is not related to the presence of the $Nd_2Fe_{14}B$ phase. When the samples annealed above 850 °C, a certain amount of $Nd_2Fe_{14}B$ magnetically hard phase appears, whereas its coercive field decreases. This result gives additional evidence to support this conclusion. At higher temperatures, the drop in H_c is not only due to the increase in the sizes of crystallite, but also due to the decomposition of metastable Fe_3B into Fe_2B and α-Fe magnetically soft phases. For the high Nd concentration samples, which contain stable phases $Nd_2Fe_{14}B$, $Nd_{1.1}Fe_4B_4$, and α-Fe, the decrease of ${}_iH_c$ is only due to the increase in the sizes of crystallite. Thus, at higher temperatures, the coercivity for the former decreases more rapidly than that of the latter.

B. The origin of hard magnetic properties

Three questions arise: (1) Where are the Nd atoms located? (2) What is the origin of the hard magnetic properties? (3) Why are three magnetic transition temperatures observed by the magnetic phase analysis in the sample annealed at 670 °C for 2 min? In order to answer these questions, we compare the difference in the HF distribution, spin-lattice and spin-spin relaxation time, and radio frequency enhancement effect between the bct-Fe_3B phases between the samples annealed at 670 and at 839 °C for 2 and 60 min, respectively.

The bct-Fe_3B phase is isostructural to tetragonal Fe_3P, in which each unit cell consists of eight formula

TABLE II. The crystallization products from the $Nd_4Fe_{77.5}B_{18.5}$ alloys after various heat treatments.

T_a(°C)	Time (min)	NMR	ME	XRD
670	2	bct-Fe_3B+α-Fe	bct-Fe_3B+α-Fe	bct-Fe_3B+α-Fe
839	60	bct-Fe_3B+α-Fe	bct-Fe_3B+α-Fe +$Nd_{1.1}Fe_4B_4$	bct-Fe_3B+α-Fe +$Nd_{1.1}Fe_4B_4$
960	60	Fe_2B+$Nd_2Fe_{14}B$ +α-Fe	Fe_2B+$Nd_2Fe_{14}B$ +$Nd_{1.1}Fe_4B_4$+α-Fe	Fe_2B+$Nd_2Fe_{14}B$ +$Nd_{1.1}Fe_4B_4$+α-Fe

TABLE III. Crystal structure and HF information for bct-Fe_3B.

Lattice parameters (Å)	Z (mol/cell)	Site	Nearest neighbor	HF (kOe) (4.2 K)	NMR frequency (MHz) (4.2 K)
$a=8.635$			10 Fe		
$c=4.285$	8	$Fe_I(8g)$	3 B	305	
			10 Fe		
		$Fe_{II}(8g)$	3 B	284	
			10 Fe		
		$Fe_{III}(8g)$	4 B	242	
		B	6 Fe 3Fe[a]		34.7

[a]These Fe atoms are farther than the nearest-neighbor Fe atoms.

units.[18,19] This phase consists of a single B site and three nonequivalent Fe sites, $Fe_I(8g)$, $Fe_{II}(8g)$, and $Fe_{III}(8g)$, with equal populations. Table III summarizes the crystal structure and HF information for bct-Fe_3B.[13,20] The Mössbauer spectrum from $Nd_4Fe_{77.5}B_{18.5}$ annealed at 670 °C for 2 min indicates that the relative intensity of the third subspectrum corresponding to the $Fe_{III}(8g)$ site in bct-Fe_3B is about 5% weaker than those from the other two. This value of 5% is much larger than the experimental error. It is commonly assumed that the recoil-free fraction is the same for the three nonequivalent iron sites in bct-Fe_3B and the relative intensity is proportional to the on-site Fe atom occupancies. This means that about 5 at. % of the Fe atoms in this site are replaced by other atoms. On the basis of the XRD, NMR, and ME results, there is no trace of the remaining amorphous Nd-rich alloys and other Nd-Fe alloys in these samples. Thus, it is reasonable to assume that some Nd atoms enter into the bct-Fe_3B lattice in the initial crystallization process. The bct-Fe_3B phase containing Nd atoms is a metastable one; when the annealing temperature is higher than 800 °C, the Nd atoms from bct-Fe_3B form the paramagnetic $Nd_{1.1}Fe_4B_4$ phase with the Fe and B atoms. For example, the sample annealed at about 839 °C for 60 min consists of bct-Fe_3B, $Nd_{1.1}Fe_4B_4$, and α-Fe. The relative intensities of the three subspectra are the same.

When fluctuations exist in the nearest-neighbor environment of the B atoms, the electronic structure of the B atoms is influenced, and consequently, the hyperfine field and its distribution at B sites is changed. Comparing the NMR spectrum from the $Nd_4Fe_{77.5}B_{18.5}$ alloys annealed at 670 °C for 2 min with that annealed at 839 °C for 60 min, it is found that the former peak corresponding to bct-Fe_3B broadens and distorts more than that of the latter. A combined NMR, ME, and XRD study demonstrates that the peak distortion is not due to the existence of orthorhombic Fe_3B. Thus, it can be assumed that this distortion may be due to Nd atoms entering into the bct-Fe_3B lattice. In order to confirm this assumption, we investigated the effect of $R=$Pr, Gd, and Dy substitution for Nd on the ^{11}B magnetic hyperfine fields for bct-Fe_3B. Figure 12 illustrates the ^{11}B HF in bct-Fe_3B as a function of R concentration x. Owing to the nonmagnetic B atoms, the contribution to the HF at the B sites in R-Fe-B compounds arises mainly from the transferred hyperfine field [THF(B)]. The THF(B) is proportional to the number of nearest-neighbor magnetic atoms and their magnetic moment.[21] For $R=$Pr, ^{11}B HF values do not increase with increasing x, but the ^{11}B resonance lines broaden asymmetrically on the high-frequency side for all samples. This may be due to the nearly equal magnetic moments for Nd and Pr. However, the substitution of Gd or Dy leads to an approximately linear increase in ^{11}B hyperfine field due to the larger magnetic moments for Dy and Gd. The ^{57}Fe hyperfine field in α-Fe was not influenced by the addition of the rare-earth elements. This gives additional evidence that some R atoms enter into bct-Fe_3B lattices. The coupling between the light rare-earth elements and Fe is ferromagnetic, while that between the heavy rare-earth elements and Fe is antiferromagnetic; both increase the hyperfine field at the B sites. This means that the R atom contribution to THF(B) comes from the rare-earth elements' magnetic moment via polarization of conduction electrons.

Table IV summarizes the spin-lattice and spin-spin relaxation times, T_1 and T_2, respectively, for the ^{11}B peaks corresponding to bct-Fe_3B obtained from $Nd_4Fe_{77.5}B_{18.5}$ alloys annealed at 670 °C for 2 min and 839 °C for 60 min. The spin-lattice and spin-spin relaxation times are deduced by measuring the spin-echo amplitude of the peaks as a function of the pulse repetition time and the interval between two pulses, respectively.[9] The very large difference in their relaxation times implies that the boron atoms are located in very different environments. For a

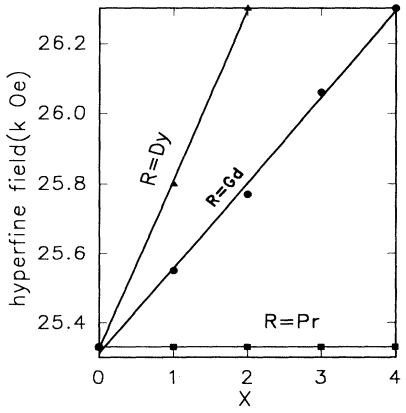

FIG. 12. ^{11}B HF in bct-Fe_3B as a function of R concentration for $R_xNd_{4-x}Fe_{77.5}B_{18.5}$ annealed at 670 °C for 2 min.

TABLE IV. The spin-lattice and spin-spin relaxation times, T_1 and T_2, for ^{11}B peaks corresponding to bct-Fe_3B under different heat-treated conditions.

Sample	T_1 (ms)	T_2 (μs)
670 °C	37	248
839 °C	130	870

nucleus with both $3d$ and $4f$ ions as the nearest neighbors, the total spin-lattice relaxation rate $(1/T_1)_{tot}$ can be written as

$$(1/T_1)_{tot}=(1/T_1)_{3d}+(1/T_1)_{4f}\ , \tag{1}$$

where $(1/T_1)_{3d}$ and $(1/T_1)_{4f}$ are the contributions from $3d$ and $4f$ ions, respectively. The spin-lattice relaxation time of bct-Fe_3B containing Nd atoms in the sample annealed at 670 °C for 2 min is much smaller than that of pure Fe_3B in the sample annealed at 839 °C for 60 min. This may result from the contribution of the near-neighbor $4f$ Nd^{3+} ions of B atoms to the spin-lattice time. The large difference for spin-lattice times between the two samples provides additional evidence that Nd atoms enter into the bct-Fe_3B lattice in the sample annealed at 670 °C for 2 min.

Table V summarizes the lattice parameters a,c and the unit cell volumes of bct-Fe_3B and α-Fe in $Fe_{81.5}B_{18.5}$ and $Nd_4Fe_{77.5}B_{18.5}$ alloys by fitting the rotation anode x-ray diffraction peaks. It can be seen that the α-Fe lattice parameter stays constant at $a=2.866$ Å with the addition of Nd, whereas the lattice constants a,c and the unit cell volumes of bct-Fe_3B containing Nd atoms in $Nd_4Fe_{77.5}B_{18.5}$ are much larger than those of pure Fe_3B in $Fe_{81.5}B_{18.5}$. The lattice expansion of bct-Fe_3B containing Nd atoms results from the substitution of larger Nd atoms (1.85 Å) for Fe atoms (1.4 Å). The x-ray diffraction patterns give a more direct evidence to support this conclusion.

It is well known that bct-Fe_3B is not desirable for a permanent magnet and $Nd_2Fe_{14}B$ is a good magnetically hard phase. Although these two phases have different structures, there is a certain relationship between the microscopic structure of bct-Fe_3B and that of $Nd_2Fe_{14}B$. In these two phase structures, each boron atom is always located in the center of a trigonal prism formed by the six nearest Fe atoms, but the scale of these prisms, and consequently, the Fe-B and Fe-Fe distances are different. Figure 13 shows the prisms of bct-Fe_3B and

TABLE V. The lattice parameters of bct-Fe_3B and α-Fe in the samples of $Fe_{81.5}B_{18.5}$ and $Nd_4Fe_{77.5}B_{18.5}$.

Samples		a (Å)	c (Å)	v (Å^3)
$Fe_{81.5}B_{18.5}$	α-Fe	2.866		23.54
	bct-Fe_3B	8.606	4.289	317.66
$Nd_4Fe_{81.5}B_{18.5}$	α-Fe	2.866		23.54
	bct-Fe_3B	8.643	4.293	320.69

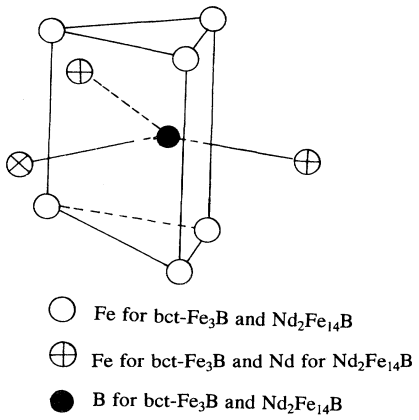

FIG. 13. The prisms of bct-Fe_3B and $Nd_2Fe_{14}B$.

$Nd_2Fe_{14}B$.[22,23] Such trigonal prisms are fundamental to the structure of many transition metal-metalloid systems, both crystalline (e.g., FeB and Fe_3C) and amorphous. In the bct-Fe_3B structure, the B atoms are located in the center of the trigonal prism formed by the six nearest Fe atoms; three other Fe atoms are situated at a slightly longer distance and bonded to each B atom through a rectangular prism face. If these three Fe atoms are replaced by three Nd atoms, the local environment of B atoms will be similar to that of $Nd_2Fe_{14}B$. Therefore, when Nd atoms enter into bct-Fe_3B, it is reasonable to suppose that bct-Fe_3B containing Nd atoms may have better hard magnetic properties owing to the large anisotropy of Nd^{3+} ions.

Since $Nd_4Fe_{77.5}B_{18.5}$ alloys annealed at 670 and 839 °C for 2 and 60 min, respectively, are multiphase materials, it is difficult to compare the magnetic properties of bct-Fe_3B containing Nd atoms and pure bct-Fe_3B directly by magnetization measurements. NMR, however, can provide information about the magnetization response of each individual phase constituent on the basis of the NMR rf field enhancement effect in magnetic materials.

There are two significant characteristics of NMR behavior in magnetically ordered materials. The first is that NMR can be observed without any external magnetic field due to the existence of the hyperfine fields in ferromagnetic materials. The second is the rf field enhancement effect. The enhancement factor can be written as[24]

$$\eta_d \propto \chi_d H_{hf}/M_s \tag{2}$$

for the domain rotation process, and

$$\eta_w \propto \chi_w H_{hf} D/(M_s \delta) \tag{3}$$

for the domain wall displacement process, where χ_d and χ_w are the susceptibilities corresponding to domain rotation and domain wall displacement, respectively. H_{hf} is the hyperfine field at the nuclei sites, M_s is the saturation magnetization of materials, D is the size of the domain, and δ is the width of domain wall.

In the spin-echo NMR experiments, the optimum rf field for maximum spin-echo intensity is determined by the following expression:[25]

$$\gamma \eta_{d,w} h_e \tau = k\pi \ , \tag{4}$$

where γ is the gyromagnetic ratio of the resonant nuclei and the constant k is determined by the pulse sequences used. For the sequence of two equal-width rf pulses, k equals $\frac{2}{3}$. τ is the width of rf pulse and $\eta_{d,w}$ is the enhancement factor for domain rotation (η_d) or domain wall displacement (η_w). The NMR behavior is associated with a parameter reflecting the "easiness" of the magnetization process, i.e., the harder the magnetization properties of the materials, the larger h_e required to excite the nuclei for maximum spin-echo signal.

Figure 14 shows the spin-echo amplitude measured for the peaks associated with the bct-Fe_3B containing Nd atoms in the sample annealed at 670 °C for 2 min as a function of the rf exciting magnetic field. For comparison, the results of the spin-echo amplitude for the peaks corresponding to pure bct-Fe_3B in the sample annealed at 839 °C are also shown in Fig. 14. The results show that the amplitude of the rf exciting field h_e required to get the maximum ^{11}B spin-echo signal from bct-Fe_3B in the sample annealed at 839 °C is only about one-third as much as that required for exciting ^{11}B in bct-Fe_3B containing Nd atoms. bct-Fe_3B containing Nd atoms has a smaller $\eta_{d,w}$, and hence, a larger coercivity than pure bct-Fe_3B. The dependence of the optimum rf field and the resonance signal intensity on the magnetic properties study has been found in previous investigations.[17,24]

Fe_3B containing Nd atoms has a lower Curie temperature than that of pure bct-Fe_3B due to the decrease of the number of Fe-Fe pairs. Thus, one can assume that the lowest magnetic transition temperature of the three magnetic transitions for $Nd_4Fe_{77.5}B_{18.5}$ annealed at 670 °C for 2 min, about 310 °C, corresponds to bct-Fe_3B containing Nd atoms, not to $Nd_2Fe_{14}B$. Thus, Mössbauer spectra at

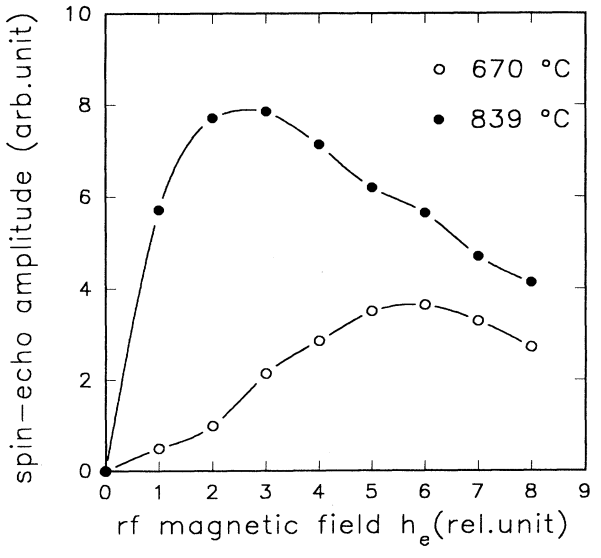

FIG. 14. The spin-echo amplitude for peaks associated with bct-Fe_3B containing Nd atoms in the sample annealed at 670 °C for 2 min and 839 °C for 60 min as a function of the excitation field.

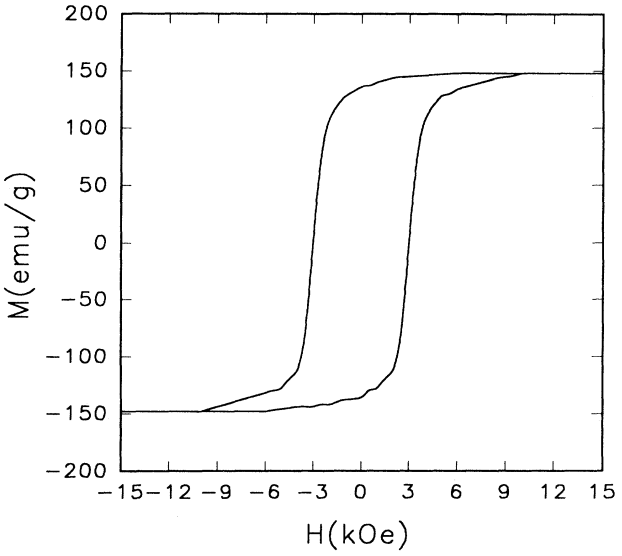

FIG. 15. *B-H* curve for $Nd_4Fe_{77.5}B_{18.5}$ crystallized at 670 °C for 2 min.

320 °C show one doublet, as performed by Li *et al.*;[26] we assume that the doublet corresponds to bct-Fe_3B containing Nd atoms. A further investigation of its magnetic properties is in progress.

Figure 15 illustrates the *B-H* curve for $Nd_4Fe_{77.5}B_{18.5}$ crystallized at 670 °C for 2 min. It has a saturation magnetization of 16 kG, and a high isotropic M_r/M_s ratio, about 0.8. The high saturation magnetization is mainly due to the presence of bct-Fe_3B, whose saturation magnetization is about 16 kG at room temperature. Although bct-Fe_3B is not a permanent magnetic phase, it exhibits a uniaxial anisotropy and anisotropy field of 4 kOe at room temperature.[27] The high coercive field state consists only of a very fine grained (about 300 Å) mixture of bct-Fe_3B containing Nd atoms and α-Fe. This phenomenon was also observed in Fe-B-Tb-La alloys,[28,29] which exhibited a high coercive field of 9 kOe, while it contained only a mixture of R_6Fe_{23} cubic phase and Fe_3B, with a small amount of α-Fe and Fe_2B also present. The strong exchange coupling between the uniaxial magnetocrystalline anisotropy bct-Fe_3B crystallite containing Nd atoms and soft magnetic α-Fe crystallite with a very fine size leads to a remanence enhancement in this material. The remanence enhancement was also found in Sm-Fe-N powders prepared by mechanical alloying methods.[30]

V. CONCLUSION

(1) The phase components crystallized under optimal conditions depend upon the Nd concentration. The samples with higher Nd concentration consist of $Nd_2Fe_{14}B$, $Nd_{1.1}Fe_4B_4$, and a small amount of α-Fe. The larger coercivity is attributed to the sizes of the $Nd_2Fe_{14}B$ crystallites below the critical size of single domain particles, and some minor phases precipitated at grain boundaries, which have a pinning domain wall effect, while the samples with lower Nd concentration do not contain $Nd_2Fe_{14}B$. The higher values of coercivity are not related

to the presence of the $Nd_2Fe_{14}B$ magnetically hard phase.

(2) The annealing temperature has a significant effect on the magnetic properties and crystallization products for melt-spun Nd-Fe-B with a lower Nd concentration. The samples annealed at 600–800 °C consist of bct-Fe_3B metastable phase and α-Fe. A paramagnetic phase $Nd_{1.1}Fe_4B_4$ appears in coexistence with bct-Fe_3B and α-Fe at 839 °C. A certain amount of $Nd_2Fe_{14}B$ only appears when the annealing temperature is higher than 850 °C, and metastable Fe_3B decomposes to Fe_2B and additional α-Fe. The drastic drop in ${}_iH_c$ is not only due to the increase in the size of the crystallites, but also due to the increase in the amount of α-Fe and Fe_2B.

(3) By comparing the ^{11}B HF distribution, Mössbauer spectra, and spin-lattice and spin-spin relaxation times for bct-Fe_3B in the sample annealed at 670 °C for 2 min with the sample annealed at 839 °C for 60 min, it can be concluded that about 5% of the iron atoms in the $Fe_{III}(8g)$ sites of bct-Fe_3B have been replaced by Nd atoms. The fact that the ^{11}B HF increases monotonically with the addition of Gd or Dy gives additional evidence for this conclusion.

(4) NMR radio frequency enhancement effect experiments demonstrate that bct-Fe_3B containing Nd atoms has a smaller enhancement factor than that of pure bct-Fe_3B, and consequently, a larger coercivity.

(5) The sample of $Nd_4Fe_{77.5}B_{18.5}$ annealed at 670 °C for 2 min shows a high M_r/M_s ratio. The remanence enhancement originates from the strong exchange coupling between the uniaxial magnetocrystalline anisotropy bct-Fe_3B containing Nd atoms and soft magnetic α-Fe with a nanoscale (about 300 Å). The hard magnetic properties are due to the existence of bct-Fe_3B containing Nd atoms.

ACKNOWLEDGMENT

This work was supported by the National Natural Science Foundation of China.

[1]K. H. J. Buschow, D. B. de Mooij, and R. Coehoorn, J. Less-Common Met. **145**, 601 (1988).
[2]R. Coehoorn, D. B. de Mooij, J. P. W.B. Duchateau, and K. H. J. Buschow, J. Phys. (Paris) Colloq. **49**, C8-669 (1988).
[3]R. Coehoorn, D. B. de Mooij, and C. de Waard, J. Magn. Magn. Mater. **80**, 101 (1989).
[4]D. Eckert, A. Handstein, K. H. Müller, R. Hesske, J. Schneider, N. Mattern, and L. Illgen, Mater. Lett. **9**, 289 (1990).
[5]K. H. Müller, J. Schneider, H. Handestein, D. Eckert, and P. Nothnagel, Mater. Sci. Eng. A **133**, 151 (1991).
[6]B. G. Shen, L. Y. Yang, J. X. Zhang, and J. G. Zhao, J. Less-Common Met. **175**, 199 (1991).
[7]M. X. Mao, C. L. Yang, Z. H. Cheng, Y. D. Zhang, B. G. Shen, L. Y. Yang, and F. S. Li, J. Phys. Condens. Matter **4**, 9147 (1992).
[8]M. X. Mao, Z. H. Cheng, C. L. Yang, F. S. Li, C. L. Zhang, Y. D. Zhang, B. G. Shen, and L. Y. Yang, J. Appl. Phys. **73**, 6980 (1993).
[9]Z. H. Cheng, M. X. Mao, C. L. Yang, Y. D. Zhang, F. S. Li, B. G. Shen, J. X. Zhang, and J. J. Sun, J. Appl. Phys. **76**, 2981 (1994).
[10]S. H. Ge, Y. D. Zhang, F. S. Li, J. I. Budnick, and P. Panissod, J. Magn. Magn. Mater. **116**, 211 (1992).
[11]O. A. Pringle, G. J. Long, G. K. Marasinghe, W. J. James, A. T. Pedziwialr, W. E. Wallance, and F. Grandjean, IEEE Trans. Magn. MAG-45, 3440 (1989).
[12]H. Onodera, A. Fujita, H. Yamamoto, M. Sagawa, and S. Hirosawa, J. Magn. Magn. Mater. **68**, 6 (1987).
[13]Y. D. Zhang, J. I. Budnick, J. C. Ford, and W. A. Hines, J. Magn. Magn. Mater. **100**, 13 (1991).
[14]G. Le Caer and J. M. Dubois, Phys. Status Solidi A **64**, 275 (1981).
[15]B. X. Gu, F. S. Li, B. G. Shen, H. R. Zhai, and S. Methfessel, Hyperfine Interact. **55**, 961 (1990).
[16]Z. H. Cheng, M. X. Mao, J. J. Sun, C. L. Yang, B. G. Shen, J. X. Zhang, F. S. Li, and Y. D. Zhang (unpublished).
[17]S. H. Ge, M. X. Mao, G. L. Chen, Z. H. Cheng, C. L. Zhang, Y. D. Zhang, W. A. Hines, and J. I. Budnick, Phys. Rev. B **45**, 4695 (1992).
[18]E. J. Lister, C. Wilkinson, T. Ericsson, L. Haggström, L. Lundgren, and R. Wapping, J. Phys. C **7**, 1344 (1974).
[19]S. Rundqvist, Acta Chem. Scand. **16**, 1 (1962).
[20]C. L. Chien, D. Musser, E. M. Gyorgy, R. C. Sherwood, H. S. Chen, F. E. Luborsky, and J. L. Walter, Phys. Rev. B **20**, 283 (1979).
[21]A. V. Zalesskij and I. S. Zheladev, At. Energy Rev. **14**, 133 (1976).
[22]P. H. Gaskell, Nature **289**, 474 (1981).
[23]J. F. Herbst, J. J. Croat, F. E. Pinkerton, and W. B. Yelon, Phys. Rev. B **29**, 4176 (1984).
[24]M. B. Stearns, Phys. Rev. **162**, 496 (1967).
[25]W. B. Mims, Phys. Rev. **141**, 499 (1966).
[26]Z. W. Li, X. Z. Zhou, A. H. Morrish, and B. G. Shen, Hyperfine Interact. **72**, 111 (1992).
[27]R. Coehoorn and C. de Waard, J. Magn. Magn. Mater. **83**, 228 (1990).
[28]N. C. Koon and B. N. Das, Appl. Phys. Lett. **39**, 840 (1981).
[29]N. C. Koon and B. N. Das, J. Appl. Phys. **55**, 2063 (1984).
[30]J. Ding, P. G. McCormick, and R. Street, J. Magn. Magn. Mater. **124**, 1 (1993).